



HAL
open science

Design of mesoscopic photonic crystal waveguides

Benedetta Ferrara, Marco Grande, Giovanna Calò, Antonella d’Orazio,
Vincenzo Petruzzelli, Béatrice Dagens, Antoine Monmayrant, Olivier
Gauthier-Lafaye, Giovanni Magno

► **To cite this version:**

Benedetta Ferrara, Marco Grande, Giovanna Calò, Antonella d’Orazio, Vincenzo Petruzzelli, et al..
Design of mesoscopic photonic crystal waveguides. *The Journal of Engineering*, 2019, 2019 (6),
pp.4628-4631. 10.1049/joe.2018.5103 . hal-02293028

HAL Id: hal-02293028

<https://laas.hal.science/hal-02293028>

Submitted on 6 Nov 2020

HAL is a multi-disciplinary open access archive for the deposit and dissemination of scientific research documents, whether they are published or not. The documents may come from teaching and research institutions in France or abroad, or from public or private research centers.

L’archive ouverte pluridisciplinaire **HAL**, est destinée au dépôt et à la diffusion de documents scientifiques de niveau recherche, publiés ou non, émanant des établissements d’enseignement et de recherche français ou étrangers, des laboratoires publics ou privés.

Design of mesoscopic photonic crystal waveguides

eISSN 2051-3305
Received on 27th June 2018
Revised 8th November 2018
Accepted on 18th December 2018
E-First on 16th May 2019
doi: 10.1049/joe.2018.5103
www.ietdl.org

Benedetta Ferrara¹ ✉, Marco Grande¹, Giovanna Calò¹, Antonella D'Orazio¹, Vincenzo Petruzzelli¹, Beatrice Dagens², Antoine Monmayrant³, Olivier Gauthier-Lafaye³, Giovanni Magno²

¹Dipartimento di Ingegneria Elettrica e dell'Informazione, Politecnico di Bari, Via Orabona 4, Bari, Italy

²Centre for Nanoscience and Nanotechnology, CNRS, Univ. Paris-Sud, Univ. Paris-Saclay, C2N, Orsay, France

³CNRS, LAAS, 7 avenue du colonel Roche, F-31400 Toulouse, France

⁴Univ. De Toulouse, LAAS, F-31400 Toulouse, France

✉ E-mail: benedetta.ferrara@poliba.it

Abstract: The authors numerically analyse the performance of a mesoscopic photonic crystal (MPhC) waveguide that could be exploited to develop a new class of routing elements and a cascaded circuitry taking advantage of the spatial and spectral reconfigurability that this structure offers. The design of the MPhC was performed by means of the 3D plane wave expansion method (3D-MPB code), while the MPhC waveguide has been analysed by a 3D-FDTD code. The numerical results show that the MPhC waveguide exhibits minimal reflections at PhC input interfaces without either affecting the feasibility or the complexity of the structure, high transmission, strong mesoscopic self-collimation and discrete translational invariance. Moreover, the influence of the characteristics of the Gaussian source on the collimation phenomenon has been explored by considering different values of the waist radius.

1 Introduction

Self-collimation (SC) phenomenon, i.e. the optical beam propagation without distortion and lateral spreading inside a structure, has become a powerful tool for different applications in alternative to the typical confining mechanisms such as index guiding and band-gap-guiding and routing. This phenomenon has been proved in photonic crystals (PhCs) [1–3] and several 2D PhC devices based on SC have been demonstrated both theoretically and experimentally as, for example, waveguides [4], cloaking [5], Mach–Zehnder interferometers [6], reconfigurable optical switch [7], splitters [8], quantum walks [9], and encoder [10]. The traditional PhC allows obtaining efficient SC only in highly symmetric direction for the lattice and not in arbitrary directions. For this reason, fixed key design parameters are required, allowing for only few degrees of freedom and extreme difficulty to combine in the same structure SC with other optical effects.

In this scenario, mesoscopic PhCs (MPhCs) have attracted the interest of research as a possible alternative of the traditional PhCs since they avoid SC limitations [11–13]. The MPhCs support the mesoscopic self-collimation (MSC) phenomenon to achieve ‘guideless’ waveguiding in linear media that can be reached by engineering their angular anisotropy [14]. A MPhC is a 1D periodic superstructure that can be realised by cascading slabs of different materials showing opposite spatial dispersion, such as traditional PhCs and slabs of bulk materials [15–17]. On the base of the spatial dispersion engineering, for a given direction, MSC is obtained when the focusing properties of the PhC slabs compensate the natural defocusing of the bulk material slabs. The ‘guideless’ waveguiding paves the way for the conception of structures showing discrete (vertical) translational invariance. In these structures a coexistence of several physical effects can occur [18, 19] that can be exploited to design a full novel class of MSC based devices, such as high sensitivity and Q-factor microcavities [20, 21], refractive index sensors [22] and optical tweezers [23, 24].

In this paper, we report on the analysis of a three-dimensional MPhC waveguide, realised by cascading PhC layers and slabs of bulk materials, considering different values of the Gaussian source waist radius (i.e. $w_0 = 10a/2, 15a/2$) in order to put in evidence the

influence of the source on the collimation phenomenon. For the optimised source waist radius w_0 equal to $15a/2$, the MPhC waveguide exhibits (i) minimal unwanted reflections at PhC input interfaces without either affecting the feasibility or the complexity of the structure, (ii) high transmission, (iii) strong MSC and (iv) discrete translational invariance.

2 Design of MPhC waveguide

The MPhC waveguide is a periodic structure realised by cascading traditional PhC layers and bulk material layers. Fig. 1 shows the sketch of the MPhC waveguide.

The 3D waveguide is realised by a 270 nm-thick GaAs membrane ($n_{\text{GaAs}} = 3.4$) fully surrounded by air. The mathematical analysis is the 3D calculation of the geometry of the single anti-reflection (AR) MPhC multilayer. To observe an AR behaviour of the MPhC, the waveguide has to show both MSC and high transmission at the same time. Therefore, the geometrical parameters of the MPhC have to satisfy the system of algebraic (1), reported in [15], where the first one represents the MSC condition while the second and the third equations represent the AR multilayer conditions:

$$\begin{cases} d_c/n_c(u) + d_b/n_b = 0 \\ d_b n_b = m\lambda/4 = ma/(4u) \\ d_c n_{\text{eff}}(u) = p\lambda/4 = pa/(4u) \end{cases} \quad (1)$$

In these equations $n_{\text{eff}}(u)$ is the PhC phase index, $n_c(u)$ is the PhC curvature index, u is the normalised frequency ($u = a/\lambda$), a is the lattice constant of the PhC, d_c is the length of the PhC slabs, d_b is the length of the bulk material slabs, n_b is the bulk membrane effective refractive index, and (m, p) are integers.

Fig. 2 shows the map of the isofrequential curves (IFCs) of the 3D-unitary cell of a square-lattice PhC characterised by a hole radius $r = 0.28 \times a$ and a lattice constant $a = 360$ nm for the first TE band, obtained by means of the plane wave expansion method (3D-MPB). The black line corresponds to the IFC showing a null

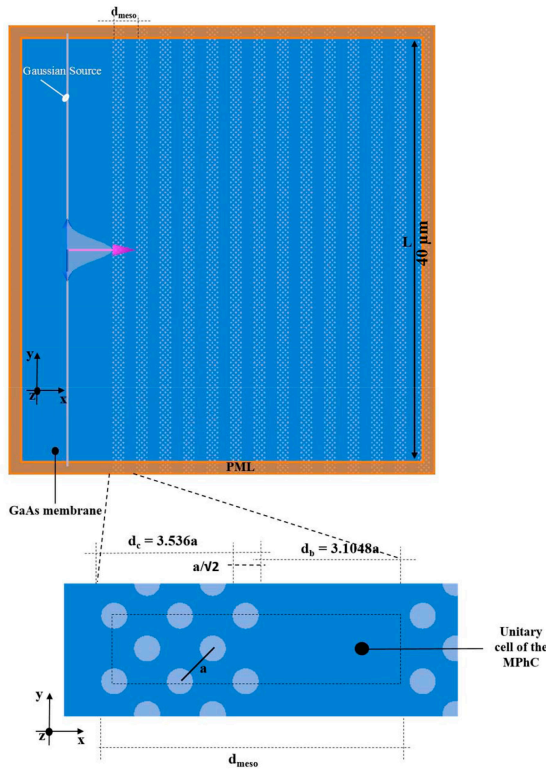


Fig. 1 (Top) Sketch of the MPhC 3D waveguide. (Bottom) The unitary cell of the MPhC

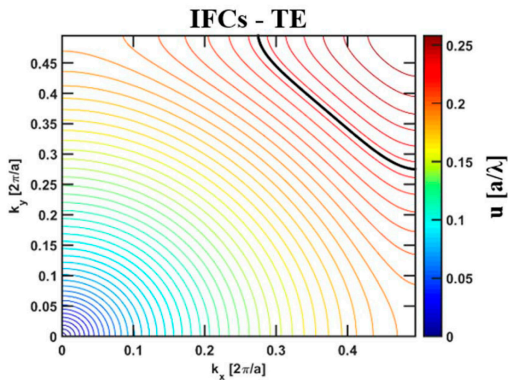


Fig. 2 IFCs-diagram of the 3D PhC unitary cell: the band diagram projected on the k -plane. The thick black curve represents the zero-curvature locus, that corresponds to the PhC self-collimation frequency

curvature. The black line, showing a flat region, corresponds to the PhC SC frequency.

Fig. 3 shows (a) the effective refractive index n_{eff} and (b) curvature index n_c , evaluated by the map of IFCs of the 3D unitary cell of a square-lattice PhC along the ΓM -direction, as a function of the normalised frequency u , calculated for the first TE band.

The evaluation of $n_{\text{eff}}(u)$ and $n_c(u)$ allows to determine the triplets (d_b, d_c, u) that satisfy the equation system (1).

Fig. 4 shows the set of retrieved solutions (d_b, d_c, u) of the equation system (1), obtained by minimising the overall error of the integer approximation for m and p . The green and red triangles represent the AR (both m and p even) and the high-reflection (HR) solutions (both m and p odd), respectively. The thick green circle highlights the AR mesoscopic PhC geometry fixed to design the MPhC waveguide.

The threshold and the frequency resolution are set equal to 0.05 and 1×10^{-7} , respectively. The mathematical analysis, i.e. the 3D calculation of the geometry of the single AR MPhC multilayer, ends once Fig. 4 is obtained. Fig. 4 allows retrieving the optimal geometry for the design of the MPhC waveguide that is based on an AR solution.

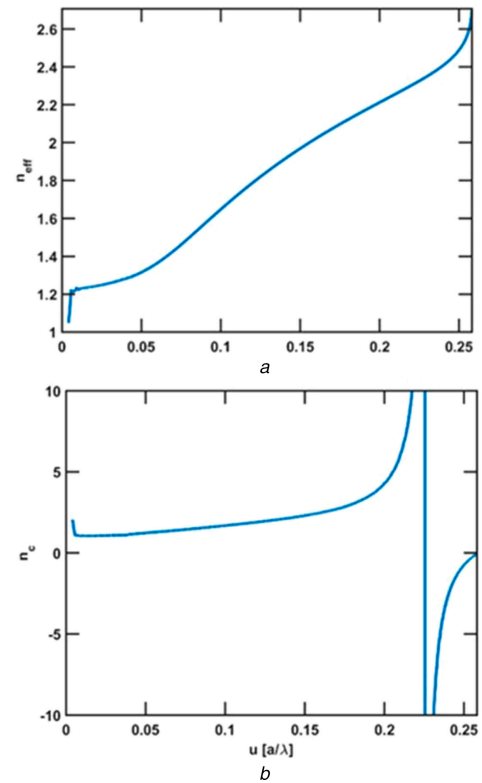


Fig. 3 Indexes

(a) Effective refractive index n_{eff} , (b) Curvature index n_c , as a function of the normalised frequency u , calculated for the first TE band of the 3D unitary cell of a square-lattice PhC

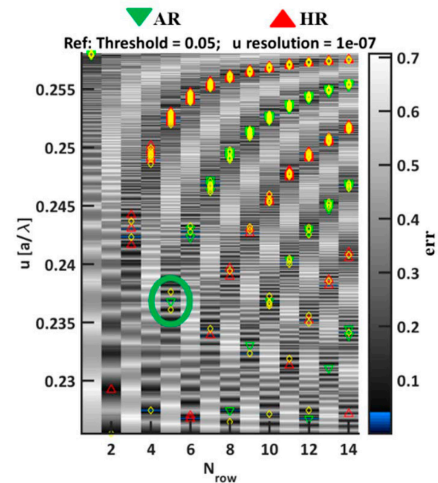


Fig. 4 Set of retrieved solutions of equation system (1), considering the 3D PhC unitary cell

In particular, we fixed $N_{\text{row}} = 5$ and, thus, the mesoperiod is obtained by interleaving focusing slab, constituted by five rows of holes of a 45° -tilted hole-type square-lattice PhC (having an overall width $d_c = 3.536 \times a$), and defocusing slab, constituted by GaAs material having width $d_b = 3.1048 \times a$. The periodic structure, having a period $\sqrt{2} \times a$, has a length equal to $40 \mu\text{m}$ along the y -direction (equivalent to 172 PhC hole rows). The waveguide is 13-mesoperiod-long along the x -direction.

The analysis of the MPhC waveguide was performed by means of 3D-FDTD calculation (Lumerical FDTD Solutions). Perfectly matched layers were imposed at the boundaries of the 3D computational cell. The structure was excited by injecting a Gaussian source ($1370 \text{ nm} < \lambda < 1670 \text{ nm}$) having a spatial distribution matching that of the fundamental TE mode (with the x -component of the electric field $E_x = 0$) of the membrane (at $\lambda = 1520 \text{ nm}$). Different values of the Gaussian source waist radius (i.e.

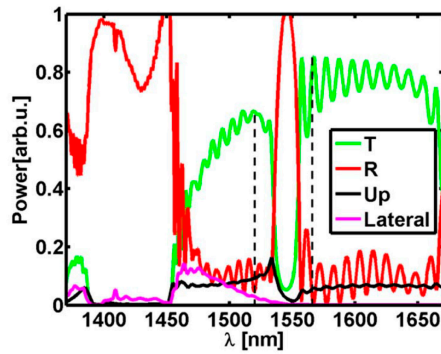


Fig. 5 Transmittance (*T*), reflectance (*R*), out-of-plane loss (*Up*) and lateral loss (*Lateral*) spectra, considering the value of the source waist radius $w_0 = 15a/2$

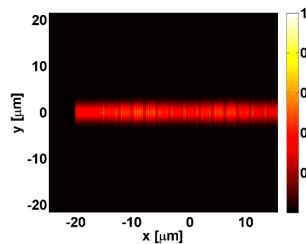


Fig. 6 Self-normalised Poynting vector at 1567 nm (linear scale), considering the value of the source waist radius $w_0 = 15a/2$

$w_0 = 10a/2, 15a/2$) have been considered in order to put in evidence the influence of the source on the collimation phenomenon.

3 Numerical results

Fig. 5 shows the transmittance (green curve) and reflectance (red curve) spectra and the out-of-plane (black curve) and lateral losses (purple curve).

The transmittance spectrum (Fig. 5) exhibits several peaks with $\sim 66\%$ transmission near the central source wavelength $\lambda_0 = 1520$ nm (black dashed line). However, the optimal performance is achieved for a wavelength $\lambda_1 = 1567$ nm with $\sim 85\%$ transmission (black dashed line) ($\approx 15\%$ smaller than the corresponding 2D-FDTD one reported in [15]), slightly above λ_0 .

A mini bandgap opens around $\lambda = 1545$ nm, corresponding to the dip appearing in Fig. 5. This is due to the overall mesoscopic-periodicity and shows a low transmission of $\sim 5\%$ ($\approx 18\%$ smaller than the corresponding 2D-FDTD one) with a slight refocusing of the beam.

When the source waist radius w_0 is assumed equal to $10a/2$, the transmittance spectrum exhibits several peaks with $\sim 62\%$ transmission near the λ_0 and the optimal performance is achieved for a wavelength $\lambda_1 = 1587$ nm with $\sim 83\%$ transmission.

As for the case $w_0 = 15a/2$, also in this last case a mini bandgap opens around $\lambda = 1545$ nm showing a transmission of $\sim 5\%$ with a slight refocusing of the beam.

In order to investigate the MSC (Figs. 6 and 7) and the influence of the out-of-plane loss (Fig. 8), the total Poynting vector was evaluated.

Fig. 6 depicts the self-normalised Poynting vector at 1567 nm (linear scale) in xy -plane, when the source waist radius is $w_0 = 15a/2$. The MPhC waveguide shows a negligible reflection at the input interface ($x = -15.78 \mu\text{m}$) when the optimised wavelength $\lambda_1 = 1567$ nm is considered. At the same time, a collimated beam over the whole structure is clearly observable. When the source waist radius w_0 is decreased down to $10a/2$ (Fig. 7), the AR MPhC waveguide, at the optimised wavelength $\lambda_1 = 1587$ nm, does not show a good collimation.

Fig. 8 shows the self-normalised Poynting vector at 1567 nm in logarithmic scale in the xz -plane when $w_0 = 15a/2$ that puts in evidence the out-of-plane losses (12%). When the source waist

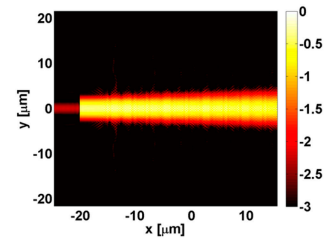


Fig. 7 Self-normalised Poynting vector at 1587 nm (logarithmic scale), considering the value of the source waist radius $w_0 = 10a/2$

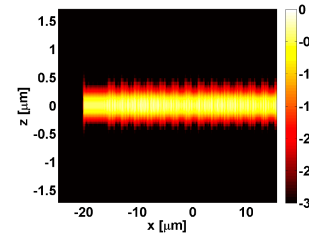


Fig. 8 Self-normalised Poynting vector at 1567 nm (logarithmic scale), considering the value of the source waist radius $w_0 = 15a/2$

radius w_0 is equal to $10a/2$, the out-of-plane loss (evaluated at the wavelength $\lambda_1 = 1587$ nm) is slightly up to $\sim 14\%$.

4 Conclusion

We analysed a 3D MPhC waveguide in GaAs considering different values of the Gaussian source waist radius (i.e. $w_0 = 10a/2, 15a/2$) in order to put in evidence the influence of the source on the collimation phenomenon. For the optimised source waist radius w_0 equal to $15a/2$, the MPhC waveguide exhibits minimal unwanted reflections at PhC input interfaces without either affecting the feasibility or the complexity of the structure, high transmission, strong MSC and discrete translational invariance.

This study opens the way for the realisation of a brand-new class of routing elements that can be combined together taking advantage of the spatial and spectral reconfigurability that these MSC-based building blocks offer. The simulated MPhC 3D waveguide could be fabricated, exploiting the MPhC cavity fabrication protocol reported in [21].

5 References

- [1] Kosaka, H., Kawashima, T., Tomita, A., *et al.*: 'Self-collimating phenomena in photonic crystals', *Appl. Phys. Lett.*, 1999, **74**, (9), pp. 1212–1214
- [2] Witzens, J., Loncar, M., Scherer, A.: 'Self-collimation in planar photonic crystals', *IEEE J. Sel. Top. Quantum Electron.*, 2002, **8**, (6), pp. 1246–1257
- [3] Rakich, P.T., Dahlem, M.S., Tandon, S., *et al.*: 'Achieving centimetre-scale supercollimation in a large-area two-dimensional photonic crystal', *Nat. Mater.*, 2006, **5**, (2), pp. 93–96
- [4] Prather, D.W., Chen, C., Shi, S., *et al.*: 'Ultralow-loss photonic crystal waveguides based on the self-collimation effect'. Proc. SPIE Photonic Crystal Materials and Devices II, San Jose, United States, January 2004, pp. 175–189
- [5] Gandji, N.P., Semouchkina, E.: 'Employing self-collimation phenomena in photonic crystals for the invisibility cloak development'. Proc. IEEE Int. Symp. Antennas and Propagation, Fajardo, Puerto Rico, June 2016, pp. 1967–1968
- [6] Chen, X., Qiang, Z., Zhao, D., *et al.*: 'Polarization beam splitter based on photonic crystal self-collimation Mach-Zehnder interferometer', *Opt. Commun.*, 2011, **284**, (1), pp. 490–493
- [7] Prather, D.W., Shi, S., Murakowski, J., *et al.*: 'Self-collimation in photonic crystal structures: a new paradigm for applications and device development', *J. Phys. D: Appl. Phys.*, 2007, **40**, (9), pp. 2635–2651
- [8] Zabelin, V., Dunbar, L.A., Thomas, N.L., *et al.*: 'Self-collimating photonic crystal polarization beam splitter', *Opt. Lett.*, 2007, **32**, (5), pp. 530–532
- [9] Qi, F., Wang, Y.F., Ma, Q.Y., *et al.*: 'Experimentally simulating quantum walks with self-collimated light', *Sci. Rep.*, 2016, **6**, (28610), pp. 1–5
- [10] Alipour-Banaei, H., Rabati, M.G., Abdollahzadeh-Badelbou, P., *et al.*: 'Application of self-collimated beams to realization of all optical photonic crystal encoder', *Physica E*, 2016, **75**, pp. 77–85
- [11] Noori, M., Soroosh, M., Baghban, H.: 'Self-collimation in photonic crystals: applications and opportunities', *Ann. Phys.*, 2018, **530**, (2), pp. 1–21
- [12] Arlandis, J., Centeno, E., Pollès, R., *et al.*: 'Mesoscopic self-collimation and slow light in all-positive index layered photonic crystals', *Phys. Rev. Lett.*, 2012, **108**, (3), pp. 037401–037404

- [13] Gauthier-Lafaye, O., Monmayrant, A., Lozes-Dupuy, F., *et al.*: 'Tailoring reflection of self-collimating multilayer structures'. Proc. ECIO, Sitges, Spain, April 2012, paper WeP048
- [14] Arlandis, J.: 'Étude de la mise en forme spatio-temporelle de la lumière dans les cristaux photoniques et les métamatériaux'. PhD thesis, Université Blaise Pascal U.F.R. Sciences et Technologies, 2012
- [15] Magno, G., Grande, M., Monmayrant, A., *et al.*: 'Controlled reflectivities in self-collimating mesoscopic photonic crystal', *J. Opt. Soc. Am. B*, 2014, **31**, (2), pp. 355–359
- [16] Magno, G., Monmayrant, A., Grande, M., *et al.*: 'Stable planar mesoscopic photonic crystal cavities', *Opt. Lett.*, 2014, **39**, (14), pp. 4223–4226
- [17] Magno, G., Monmayrant, A., Grande, M., *et al.*: 'Self-collimation in mesoscopic photonic crystals: from reflectivity management to stable planar cavities'. Proc. 16th ICTON, Gratz, Austria, July 2014, pp. 1–4
- [18] Monmayrant, A., Lozes-Dupuy, F., Gauthier-Lafaye, O., *et al.*: 'Multifunctional self-collimating mesoscopic photonic crystals'. Proc. CLEO Europe/IQEC, Munich, Germany, May 2013, pp. 1–1
- [19] Magno, G., Monmayrant, A., Grande, M., *et al.*: 'Mesoscopic self-collimation: beyond the high symmetry constraint'. Proc. CLEO Europe, Munich, Germany, June 2015, OSA, paper CKP31
- [20] Magno, G., Monmayrant, A., Grande, M., *et al.*: 'Stable planar microcavities based on mesoscopic photonic crystals'. Proc. SPIE Integrated Optics: Devices, Materials, and Technologies XVIII, San Francisco, United States, February 2014, pp. 89881G-1–89881G-10
- [21] Monmayrant, A., Grande, M., Ferrara, B., *et al.*: 'Full optical confinement in 1D mesoscopic photonic crystal-based microcavities: an experimental demonstration', *Opt. Express*, 2017, **25**, (23), pp. 28288–28294
- [22] Ferrara, B., Grande, M., Calò, G., *et al.*: 'Optical sensor based on a mesoscopic photonic crystal microcavity'. Proc. Conf. ACP, Wuhan, China, November 2016, OSA, paper AS3H.5
- [23] Ferrara, B., Grande, M., Calò, G., *et al.*: 'Design of mesoscopic photonic crystal microcavity based sensors devoted to optical tweezing applications'. Proc. XXI RiNEM, Parma, Italy, September 2016, pp. 264–267, ISBN: 978-88-907599
- [24] Ferrara, B., Ecarnot, A., Monmayrant, A., *et al.*: 'Optical trapping in 1D mesoscopic photonic crystal microcavities'. Proc. SPIE Photonics Europe 2018, Strasbourg, France, April 2018, pp. 106721E-1–106721E-7